Available online at www.sciencedirect.com
ScienceDirect
Cement and Concrete Research 36 (2006) 1708–1718
Cement and Concrete Research

Microstructure-based micromechanical prediction of elastic properties in hydrating cement paste

Vít Šmilauer *, Zdeněk Bittnar

CTU in Prague, Civil Engineering, Department of Mechanics Thákurova 7, 166 29, Prague 6, Czech Republic

Received 7 April 2005; accepted 19 May 2006

Abstract

Elastic properties of hydrating cement paste can be successfully predicted by combination of the hydration model, percolation theory and micromechanical analysis. Reconstruction of hydrating microstructure is based on the 3D digital NIST model of cement hydration, which is enhanced for the prediction of two C–S–H types. Chemical phases in a percolated microstructure served as an input in a two-level analytical or one-level 3D FEM or FFT elastic homogenization. Special mesh generation for the percolated microstructure is discussed as well as its numerical implementation. Good results from FEM and FFT were found for the size of the representative volume element of $50 \times 50 \times 50$ μm, considering water-to-cement ratio in the range from 0.25 to 0.5. While good predictions in well-hydrated cement pastes were obtained for both analytical and numerical approaches, numerical homogenization was found more accurate and versatile for the whole hydration time.
© 2006 Elsevier Ltd. All rights reserved.

Keywords: Cement paste microstructure; Elastic homogenization; Elastic moduli; Hydration; Hydration products; Finite Element Analysis

1. Introduction

Young's modulus (E) and Poisson's ratio (v) are important parameters used in the structural design and analysis of cement-based materials. Physical and chemical changes in the microstructure of cement paste result in the evolution of mechanical properties. While porosity determines the strength to a great extent, elastic properties depend on the intrinsic elastic values of individual components and their connectedness [3]. Therefore, modification of elastic behavior is a challenge that finds its application in large-span structures, for example.

Several macroscopic approaches were aimed at the description of the evolution of Young's modulus, based on the maturity concept, degree of hydration [22], or percolation [5,31]. Moreover, linear dependence between the degree of hydration and Young's modulus was reported several times [8,24]. The next consecutive step deals with volumetric prediction of dominant chemical phases via microscale models of cement hydration, combined with the homogenization approach. Here, previous macroscopic results are very useful for validation. Volumetric fractions from continuous affinity hydration models may provide such input for analytical homogenization [3]. Although the analytical homogenization relies on morphological assumptions and does not account for true microstructure configuration, the results were adequate [3]. More sophisticated, direct homogenization via FEM from a discrete hydration model also yielded good results, even for leached cement pastes [9,12,16]. Convergence of analytical and numerical homogenization methods is generally observed at later stages of hydration where porosity and percolation do not play a significant role.

The homogenization approach is complicated by the fact that cement paste starts as a suspension and a load-bearing structure emerges only after a setting time period. Percolation theory partially addresses this phenomenon near to the set point. Non-critical application of percolation theory to later evolution of microstructure is problematic since a big gap in elastic properties exists between raw cement and hydration products and a certain correction is necessary [31]. Alternatively, the use of contact finite elements have recently been shown to solve this problem [29]. The aim of this paper is to relate effective elastic properties of cement paste to the properties of its individual chemical phases on the nano- and micro-level, using methods of uncoupled upscaling [3]. The percolation threshold, which

* Corresponding author. Tel.: +420 224 355 417; fax: +420 224 310 775.
E-mail address: vit.smilauer@fsv.cvut.cz (V. Šmilauer).

0008-8846/$ - see front matter © 2006 Elsevier Ltd. All rights reserved.
doi:10.1016/j.cemconres.2006.05.014

defines the transition from a suspension to a partially solid structure, is determined from the NIST cement hydration model working on the micrometer scale [2]. The model further serves for estimating the chemical composition and spatial configuration of the microstructure which will provide an input to two-level analytical or one-level numerical homogenization.

2. Cement hydration model CEMHYD3D

The discrete hydration model, called CEMHYD3D and developed at NIST, will be used for the reconstruction of 3D cement microstructures; for details see [2,10]. The model reflects four important effects during cement hydration: cement chemical composition, particle size distribution (PSD), curing regime and temperature. A voxel (volume element) is the basic building unit and represents one chemical phase. The size of the voxel determines the model resolution that should be small enough to capture the important underlying processes, e.g. dissolution, transport, reaction, and diffusion. A reasonable voxel size of $1\times1\times1$ μm has been found [10]. Basic chemical reactions guarantee the correct volume fractions of hydrating Portland cement.

An initial and random 3D microstructure is reconstructed with the help of autocorrelation functions and contains typically four cement clinker minerals and forms of calcium sulfate, all as digital spherical particles [2]. Hydration products are, with certain probabilities, formed on the grains exposed to water contact and they nucleate in the available pore space. The size of microstructure may be arbitrary, limiting the maximal cement grain that may be placed in. The microstructure remains periodic during hydration which enables homogenization techniques dealing with periodic fields. Although the real hydration time may be determined from the model, the degree of hydration is preferred, in order to avoid the fitting parameter related to the model cycles [2].

Any random model system contains two sources of error: statistical fluctuation and the finite size effect [10]. The first emerges due to the random nature of cement paste while the second is due to limited representation of a sample. Comparison of various sizes of hydrating microstructures gives an estimate of the expected error. It has been shown that for water-to-cement ratio (wcr) from 0.2 to 0.5, for fine and coarse cement, and for an expected error in the degree of hydration of 10% at the same model cycle after 3 h of hydration, the reasonable microstructure size lies in the range of 20–50 μm [23]. A microstructure edge size above 100 μm has been found to bring no significant accuracy in the hydration model predictions in terms of released heat [10].

This model of cement hydration also brings digital resolution problems. The voxel is likely to lie in the range from 0.125 to 1 μm/voxel and has been determined using an assumption of continuous C–S–H phase and a dissolution rate of larger cement grains [10]. The progress of the reaction front towards a grain is also influenced by a dissolution length, specified as 6 or 26 adjacent voxels. The latter value corresponds to a $3\times3\times3$ voxel box around the central voxel and specifies candidates to be dissolved. Although the dissolution length significantly changes the hydration kinetics, the elastic results remain less sensitive as demonstrated in the validation section.

2.1. Models for two morphologies of C–S–H gel

It has been observed over the past decades that the C–S–H gel, as the main hydration product, may be divided into two groups called inner–outer [21], middle–late product, phenograins–groundmass, low–high density (C–S–H_{LD} – C–S–H_{HD}) [15,26]. Though these pairs of expressions are not equivalent, they are closely related. According to the Jennings–Tennis (J-T) model, a globule with a diameter around 5 nm is probably responsible for the two types of C–S–H gels [15].

It is believed that at the beginning of hydration only C–S–H_{LD} appears due to unrestrained pore space while C–S–H_{HD} originates from later stages of cement hydration when diffusion reactions dominate in the microstructure. This transition happens at the nanometer scale. Our first attempt to model this change in the voxel-based model has been based on an explicitly given transition thickness, which roughly defines the change to the C–S–H_{HD} in a given neighborhood around a cement grain. It has been found that the results are almost independent of the cement fineness and of the wcr, which is in contradiction to the J-T model [26].

A more successful model distinguishing two morphologies of C–S–H has been based on a confinement condition. At the beginning of hydration, there is enough capillary space to accommodate C–S–H; hence, it is of the C–S–H_{LD} type. As hydration proceeds, expanding solid phases are more restrained, causing compressive stresses. It is assumed that these stresses transform C–S–H_{LD} to the C–S–H_{HD} type. This mechanism results in an algorithm:

1. locate an undifferentiated C–S–H voxel from CEMHYD3D model,
2. determine the amount of all solid voxels in a box around the monophase C–S–H voxel,
3. if the amount equals at least to a transition one, change all C–S–H voxels in the box to C–S–H_{HD} type,
4. scan the next C–S–H voxel in the microstructure.

Two unknown parameters have to be determined for this confinement model: the box size around the C–S–H voxel and the amount of solid voxels in that neighborhood to cause the transition. For the purpose of parametric study, three OPC microstructures with a wcr of 0.2, 0.3 and 0.5 have been generated. Fig. 1 displays the results of the C–S–H_{HD} evolution, where the straight lines correspond to the J-T model [26]. There are also results for the evolution of C–S–H_{HD}, assuming the amount of 26 solid voxels in the box of $3\times3\times3$ around the C–S–H voxel. If the box $5\times5\times5$ is considered, a transition amount of 119 solid phases yields the closest match to previous results. Similar results were found for different wcrs suggesting that a larger box or optimisation of the algorithm is not necessary.

The $3\times3\times3$ box with 26 solid voxels seems to be the most reasonable choice, used also later throughout validation. This

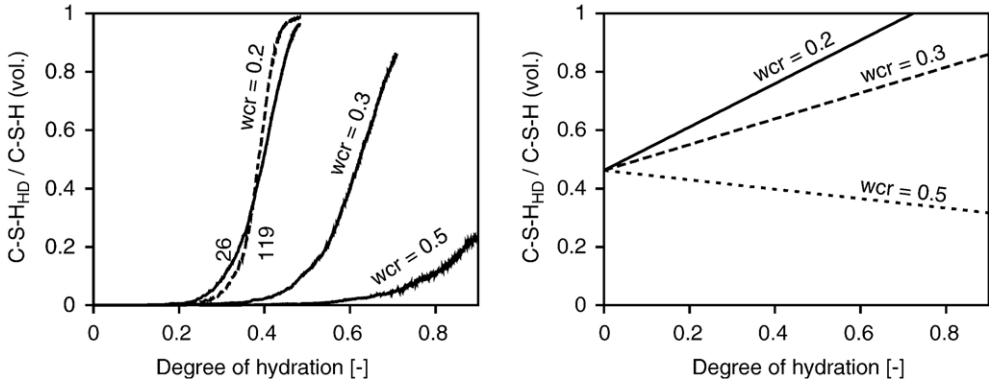

Fig. 1. C–S–H_{HD} evolution for three wcrs based on the confinement model (left) and based on the J-T model (right) [26].

choice is supported by the J-T model [26], where the volumetric C–S–H_{HD}/C–S–H ratio for the ultimate degree of hydration is supposed to be 0.8 and 0.5 for the wcr of 0.25 and 0.4, respectively. The data from the affinity model also support this choice [3]: C–S–H_{HD} starts to form at the degree of hydration of 0.6 at wcr = 0.6 and the volume fraction of C–S–H_{HD} is around 30% at a degree of hydration of 0.9.

The assumption of C–S–H_{HD} origin in rather later diffusion processes leads to obvious disagreement in Fig. 1 when compared to the J-T model. On the other hand, the J-T model is extrapolated to early ages where surface area determination brings difficulties [26]. However, the question of early C–S–H_{HD} evolution remains open and the confinement model will be used exclusively for the purpose of elastic homogenization. It must be further noted that implementation of two different molar volumes of both C–S–H gels may be necessary to improve the model. When interstitial space in the C–S–H is filled with water, the densities of both types were calculated as 1850–1980 or 2037–2195 kg/m^3, depending on the density of globules [15]. The confinement model exhibits a weak dependence on the resolution since only "surface" layers of C–S–H are affected by the resolution and the C–S–H_{HD} remain in the close vicinity of the cement grains.

2.2. Percolation concept

Percolation theory describes topological connection in a random material of at least two phases. There exists a strong link between the behavior of a random material and percolation, e.g. elasticity, conductivity, permeability [28]. When applied to cement paste, percolation of solids p, further referred to as percolation, is quantified as

$$p = \frac{\text{connected volume of solids}}{\text{total volume of solids}}. \quad (1)$$

In the beginning of hydration, the cement grains are mutually separated hence connected volume fraction and percolation of solids is equal to zero. As hydration proceeds, the hydration products glue the grains. At the point called the percolation threshold of solids p_c, the microstructure contains sufficient amount of solids to bridge one side to the opposite.

Fig. 2 shows an example of 2D microstructure from the NIST model, containing digital spheres of cement grains, porosity and hydration products acting as a glue. In such digital images, two voxels are considered to be connected when they share the same face and do not belong to different cement grains [10]. For this purpose, the NIST authors implemented the "burning" algorithm that locates all solid phases that bridge opposite sides of the microstructure [2]. In Fig. 2, the microstructure has already attained the percolation threshold where spanning and isolated clusters may be identified.

For a statistically homogeneous material, the static Young's modulus attains a non-zero value only after the percolation threshold p_c has been reached [5,28]. In other words, appearance of the first spanning cluster over the microstructure is a necessity. Several studies of hydrating cement pastes from the NIST model revealed that the percolation threshold

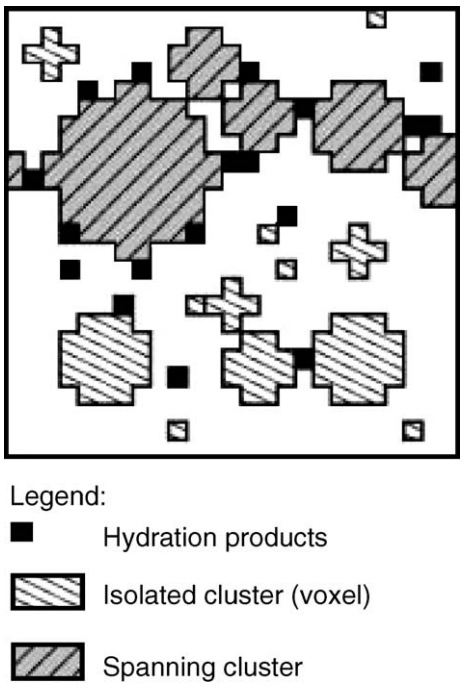

Fig. 2. Example of 2D cement microstructure shortly after the percolation threshold of solids, emphasizing their percolation.

corresponds to the percolation in the range from 0.2 to 0.6, depending on the model resolution [2,10]. In the vicinity of the percolation threshold, the static Young's modulus obeys the power law:

$$E(p) = k(p-p_c)^f, \quad (2)$$

where f is the critical exponent and k is the structure parameter. Numerical simulations of a 3D random material network yield $f = 3.75$ [28].

Ye et al. [31] used the same structure of Eq. (2) for determination of the shear modulus of cement paste. They obtained parameters $f = 1.35$, k on average as 27 GPa and $p_c \sim 0.4$ for the OPC with the wcr = 0.5 and 0.6 [31]. They concluded that the percolation threshold seems to be independent in these two wcrs. Boumiz et al. [5] found good correlation with shear modulus for f in the range from 1.92 to 2.13 for the wcr between 0.34 and 0.4. It must be noted that Eq. (2) is valid only in the vicinity of the percolation threshold, i.e., at the initial stages of cement hydration, and does not take into account the significant change of elastic properties of phases during chemical reactions, Table 1.

It is obvious that isolated clusters do not contribute to the shear stiffness. Until the first spanning cluster appears, the mechanical behavior resembles that of water. Therefore, the substitution of isolated voxels with water-filled porosity is necessary while leaving the spanning clusters of solids. The term *percolated microstructure* will refer further to such configuration.

3. Homogenization of cement paste

A lot of literature deals with the theory of homogenization, a brief review is given in, e.g., [27,32]. Generally, three types of micromechanical methods are used. *Rigorous bounds* such as the Hashin bounds, *analytical approximations* such as the self-consistent scheme, differential medium or third-order approximations, and *numerical methods* like finite elements [25], boundary integrals, Fourier transforms [20] or method of cells.

The transition from a heterogeneous to a homogeneous material at higher level requires statistically homogeneous material, in other words, an appropriate size of a sample called representative volume element (RVE). Generally, the size of the RVE is a function of five parameters: the analyzed physical quantity, the contrast of material properties, the volume fraction of components, the relative error and the amount of realizations of random microstructure [17].

The selection of RVE in a cement paste depends not only on the morphology but also on the data available on the identification of the intrinsic properties of constituents. The smallest mechanical tests were performed via nanoindentation on the nanometer scale. This is the smallest considered level, referred to as the C–S–H level [3]. According to Jennings's model [15], the characteristic length of packed globules ends at 100 nm. This length scale contains also inclusions of C–S–H gel porosity and small calcium hydroxide crystals that can be hardly separated from the matrix during nanoindentation tests.

The higher level, referred to as the cement paste level, spans the characteristic length approximately from 1 μm up to 100 μm. The upper limit depends especially on the maximum size of cement grain used in calculation. The cement paste level contains four unhydrated cement clinkers (C_3S, C_2S, C_3A, C_4AF), gypsum, larger calcium hydroxide crystals, ettringite, capillary porosity, other minor phases and already homogenized C–S–H phase. The RVE of this level corresponds to the representative cube from the NIST model, typically in the range from 25 to 100 μm.

The homogenization approach is easily applicable to coarser scales, arriving to mortar and concrete level with the characteristic length up to 0.1 m, covering the range of several orders of magnitude [3].

3.1. Intrinsic elastic properties of chemical phases

With the development of nanoindentation, elastic properties of constituents can be accessed at very fine scales, typically in the range from 300 to 500 nm. Synthetically prepared clinker minerals (C_3S, C_2S, C_3A, C_4AF) were analyzed via nanoindentation and by the resonance frequency technique [30], Table 1. Higher scatter of values from nanoindentation reflects also higher intrinsic porosity. It is assumed that all reactants and products keep their specific elastic properties constant during the whole cement hydration. Constantinides and Ulm [6] performed nanoindentation tests of C–S–H and calcium hydroxide, in an OPC with the wcr of 0.5. They found two peaks in Young's modulus that may be probably attributed to the C–S–H_{LD} and C–S–H_{HD} type, Table 1. Since these three constituents are the most common hydration products, effective properties of the cement paste rely considerably upon their elastic behavior.

The Poisson's ratio of water strongly influences the resulting Poisson's ratio during the early hydration period [3]. The question remains as to whether the water can move in reality without any constraint through the capillary network. If so, the

Table 1
Intrinsic elastic moduli of chemical phases in the homogenization as measured by nanoindentation or mechanical tests

Phase	E (GPa)	ν (–)	Reference
C_3S	**135**±7	**0.3**	[30]
C_2S	**130**±20	**0.3**	[30]
C_3A	**145**±10	**0.3**	[30]
C_4AF	**125**±20	**0.3**	[30]
$C\bar{S}H_2$	16–**30**–35	0.18–**0.3**–0.34	[1]
Water-filled porosity	**0.001**	**0.499924**	–
Empty porosity	**0.001**	**0.001**	–
CH	**38**±5	**0.305**	[3,6]
C–S–H_{LD}	**21.7**±2.2	**0.24**	[6]
C–S–H_{HD}	**29.4**±2.4	**0.24**	[6]
$C_6A\bar{S}_3H_{32}$	**22.4**	**0.25**	[16]
$C_4A\bar{S}H_{12}$	**42.3**	**0.324**	[16]
C_3AH_6	**22.4**	**0.25**	*
FH_3	**22.4**	**0.25**	*

Bold values enter the homogenization procedure, values denoted by asterisks are estimated, based on [16].

water should act in the micromechanical model as an easily compressible void. This problem emerges in analytical homogenization since there is no information about percolation of the capillary network. On the other hand, numerical homogenization localizes the deformation in empty capillary pores in the RVE since the connectivity of capillaries is given by phases arrangement. Assigning a non-zero Young's modulus to water, Poisson's number is determined in such a way that the bulk modulus of water corresponds to $k = 2.18$ GPa.

3.2. Analytical approximation

Two level analytical homogenization, proposed by Bernard et al. [3], will be applied in order to verify the assumptions of analytical methods against the numerical results. The Mori–Tanaka method [19] homogenizes the C–S–H level, where the C–S–H_{LD} is the reference phase. The cement paste level is homogenized by the self-consistent scheme [13]. In the latter, the percolation threshold of solids coincides with the porosity of at least 50%, depending on assigned elastic properties of porosity [3].

3.3. Numerical approximations and boundary conditions

The microstructure configuration is a prerequisite for numerical methods, here obtained from the NIST hydration model. The finite element method (FEM) provides a robust tool for arbitrary RVE, material properties, and boundary conditions (b.c.). In our case, the RVE has the shape of a cube, where one voxel corresponds to one finite element. A brick element with tri-linear shape functions was found appropriate [9]. Recently, a new homogenization method of periodic composites has been introduced, based on fast Fourier transformations (FFT) [18,20]. The FFT homogenization in the discrete form may be considered as a kind of FEM with good enough approximation functions. Therefore, the mesh refinement makes no improvement of results, as opposed to FEM. The FFT homogenization will serve here only as an indicator of error obtained from FEM.

Drugan and Willis [7] showed that the RVE size should be approximately two sphere diameters for a random distribution of identical spheres in the case of elastic response. Gusev [11] carried out a 3D FEM study on identical spheres in a matrix, where the spheres occupied approximately 26% of volume and the modulus contrast was around 20. He found the optimum RVE size was around 3–5 times the sphere diameter. Similar results have been obtained by Zeman and Šejnoha [33] for analysis of real-world materials. Böhm and Han [4] reported that relatively small RVE sizes can be used for apparent elastic moduli but non-linear behavior required much larger sizes. Though these findings are not directly applicable to the case of a cement paste, results from the validation section are consistent.

The RVE may be subjected to three basic types of load: displacements, tractions, or periodic boundary conditions. Kinematic uniform boundary conditions (KUBC) are prescribed as displacements u at the boundary Γ of RVE:

$$u = E \cdot x, \quad \forall x \in \Gamma, \tag{3}$$

where x is a coordinate tensor and E represents the macroscopic prescribed strain tensor. Static uniform boundary conditions (SUBC) are imposed as prescribed tractions σ on Γ:

$$\sigma \cdot n = \Sigma \cdot n, \quad \forall x \in \Gamma, \tag{4}$$

where n is the normal to Γ at x and Σ is the macroscopic prescribed stress tensor.

The periodic boundary conditions mean in our case that the opposite sides of the RVE share the same displacements. Homogeneous strains are imposed over all finite elements to load such RVE:

$$\boldsymbol{F}^e = \int_V B^T D T \mathrm{d}V, \tag{5}$$

where $\boldsymbol{F}^e$ is the node force vector of the element, B is the strain interpolation matrix, D is the material stiffness matrix and T is the matrix containing macroscopic prescribed strains.

After assembling the global stiffness matrix K and node forces $\boldsymbol{F}$, the reduced equation is solved with the conjugate gradient method:

$$K\boldsymbol{r} = \boldsymbol{F}, \tag{6}$$

where the vector $\boldsymbol{r}$ contains node displacements.

Similar NIST code with the conjugate gradient method has already been used for an analysis of cement pastes [9]. Presented algorithms have been implemented in an open-source FEM software[1], allowing an arbitrary mesh structure. The results for special RVE were compared with exact analytical results, e.g., two phase random material with equal shear moduli, serial and parallel layers, or small contrast in material properties [9].

The response of the RVE is not necessarily isotropic due to statistical inhomogeneity such as early percolation. Averaging is performed, assuming the same accumulated mechanical energy W in anisotropic and isotropic material in the equilibrated RVE:

$$W = \frac{1}{2}\langle \boldsymbol{\epsilon} \rangle \ : \ \langle \sigma \rangle = \frac{1}{2}\langle \boldsymbol{\epsilon} \rangle \ : \ C_{\mathrm{iso}}^{\mathrm{hom}} \ : \ \langle \boldsymbol{\epsilon} \rangle, \tag{7}$$

where $C_{\mathrm{iso}}^{\mathrm{hom}}$ is the stiffness tensor of the isotropic material, $\langle \boldsymbol{\epsilon} \rangle$ and $\langle \sigma \rangle$ are the volume averages of strain and stress tensor over RVE, respectively.

Huet [14] and Kanit et al. [17], among others, showed that KUBC result in higher apparent effective moduli, if the RVE is insufficiently small. On the other hand, SUBC lead to considerably lower apparent effective moduli:

$$C_{\mathrm{SUBC}}^{\mathrm{app}} \leq C_{\mathrm{PERIODIC}}^{\mathrm{app}} \leq C_{\mathrm{KUBC}}^{\mathrm{app}}. \tag{8}$$

Kanit et al. [17] found that the bias of apparent properties is the lowest for the periodic boundary conditions when the RVE size changes. However, when the RVE is large enough, all three boundary conditions yield the same result.

[1] SIFEL–SImple Finite ELements. Open-source package. http://cml.fsv.cvut.cz/~sifel.

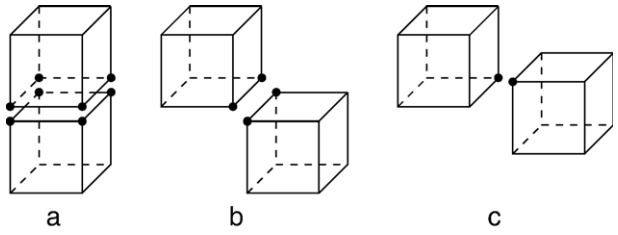

Fig. 3. Possible configuration of split nodes in solid adjacent voxels.

3.4. Mesh generation for FEM

The simplest mesh is an equally spaced, uniform grid, where one voxel corresponds to a brick element in the form of a cube [9]. Preliminary simulation with only spanning clusters revealed that the early-hydrated RVEs are too stiff when compared to experimental data. The reason is in different contact type between percolation and FEM; while percolation takes into account a connection face-to-face, FEM works on common displacements at nodes. It may happen that two adjacent brick elements are in a spanning cluster, they share the same nodes but belong to different cement grains, for example. In such a case, the common displacements are separated in order to reduce the stiffness of the RVE. A split node is introduced, which replaces to some extent the contact elements and relax concentrated stresses as well. The RVE with *split node* contains only spanning clusters where the water-filled porosity substitutes isolated voxels.

Consider any inner node in the RVE. Eight finite elements intersect in that node and all share the common displacement. To disconnect certain elements from that node, three possible configurations exits, Fig. 3. Disconnection by a face (Fig. 3a) needs additional 4 nodes, by an edge 2 nodes (Fig. 3b), and by a vertex 1 node (Fig. 3c). Note that each node has three degrees of freedom. Under practical simulations, the total amount of nodes in the RVE increases up to 15% due to the introduction of the split node.

Accuracy improvement is possible on the cement hydration model as well as in the part of numerical homogenization. Refinement of the mesh within the same RVE will verify only FEM performance. Better results are expected when the hydration model refines the voxel size and consequently the mesh, maintaining one finite element per one voxel. After that,

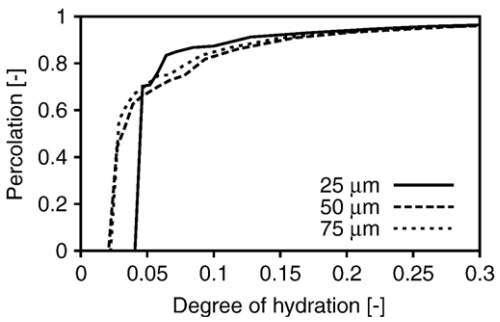

Fig. 4. Effect of RVE size on percolation of solids, wcr = 0.5.

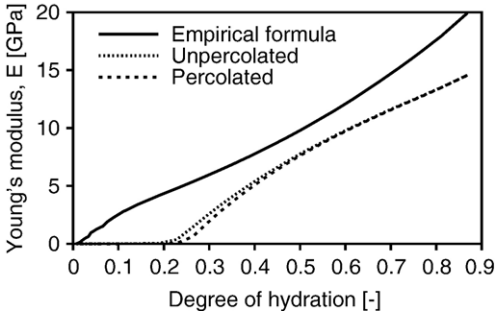

Fig. 5. Young's modulus predicted from analytical homogenization, un/percolated RVE, wcr = 0.5.

the results reflect the role of RVE size and numerical homogenization performance.

4. Validation and discussion

Many experiments demonstrate that the modulus of elasticity is almost directly proportional to the degree of hydration [5,16]. Cement pastes with a wcr in the range from 0.25 to 0.5 were validated analytically and numerically, covering the range routinely used in practice. The cement image reconstruction was based on the autocorrelation functions from the NIST cement database and the PSD was approximated from the Blaine fineness [2,23].

4.1. Loose cement paste, wcr = 0.5

The first example covers ordinary CEM I, wcr = 0.5, based on the work of Kamali et al. [16]. They approximated the evolution of E modulus with the function:

$$E = 46.03(1-f_{\text{cap}})^{3.16}, \tag{9}$$

where f_{cap} is a volume fraction of the capillary porosity from the NIST model, decreasing during hydration. In this case, f_{cap} is calculated from the percolated RVE and is equal to one until the percolation threshold of solids is reached.

In order to explore an effect of the RVE size, three samples with edge lengths of 25, 50, 75 µm were generated using the same PSD curve and autocorrelation functions [16]. The voxel edge and the resolution are 1 µm and each representative cube

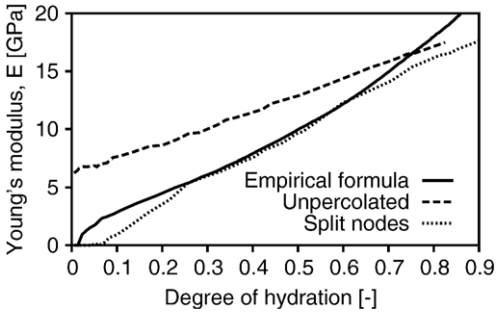

Fig. 6. Effect of percolation on E modulus, 25 × 25 × 25 µm, FEM–periodic b.c., wcr = 0.5.

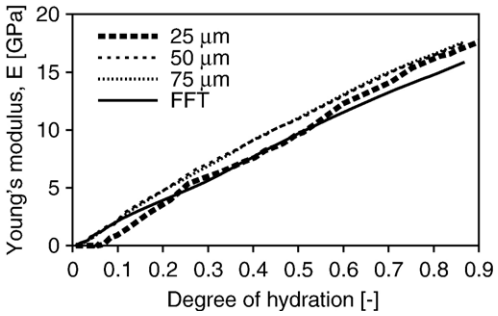

Fig. 7. Effect of RVE size on E modulus, FEM–periodic b.c., split nodes, FFT, wcr = 0.5.

contained the largest possible cement grain, i.e., the diameter of half of the RVE. The NIST model ran 1500 cycles at a constant temperature 20°C for each case with the dissolution box of $3\times3\times3$ μm. Fig. 4 displays percolation for one principal direction at early ages, determined as the connected volume fraction of all solid phases. It is obvious that a larger cement grain fills the pore space better than smaller grains. Therefore, the larger RVE percolates sooner but when the hydration degree exceeds approximately 0.15, the percolation falls nearly on the same curve.

Fig. 5 shows the E modulus as predicted from the two-level analytical homogenization. The volume phase fractions were taken from the RVE of 75 μm either as unpercolated or percolated. The high final capillary porosity of this paste, 23% at the degree of hydration of 0.87, makes the prediction less accurate and modulus underestimation is typical for the self-consistent scheme at the cement paste level [3].

Fig. 6 demonstrates an effect of percolation on Young's modulus, as calculated via the FEM with periodic boundary conditions, in the RVE of 25 μm. An unpercolated RVE with the regular mesh yields non-zero apparent moduli from the beginning of hydration. The reason has already been explained and percolated RVE with split node is remedy.

Fig. 7 displays the effect of RVE size with split nodes, using previous RVEs with percolated phases. While the edge size of 25 μm is too small and leads to stiffness underestimation at early ages, the difference between 50 and 75 μm size is negligible and the results correspond well to empirical formula Eq. (9). The FFT method of the 75 μm RVE predicts comparable values with the FEM. Note that FFT method does not allow the split node algorithm and in this case contains only percolated phases in the RVE. On the other hand, the stress concentration at sharp corners is treated exactly.

The effect of RVE size on the apparent elastic properties was explored on the RVEs with the edges of 10, 25, 50, 75 and 100 μm. Since the placement of digital spheres in initial cement image is per se random, five RVEs from each size, with different spatial configuration, were evaluated. The same dissolution box $3\times3\times3$ μm was used during all simulations.

Fig. 8 shows the E moduli from FEM with three types of boundary conditions at the degree of hydration of 0.3 and 0.9. The bars represent the 95% confidence level from five random simulations at each size. Both figures follow bounds from inequality (8). Periodic boundary conditions exhibit the lowest dependence on the RVE size and the size of 50 μm seems to be representative enough. However, going to earlier stages of

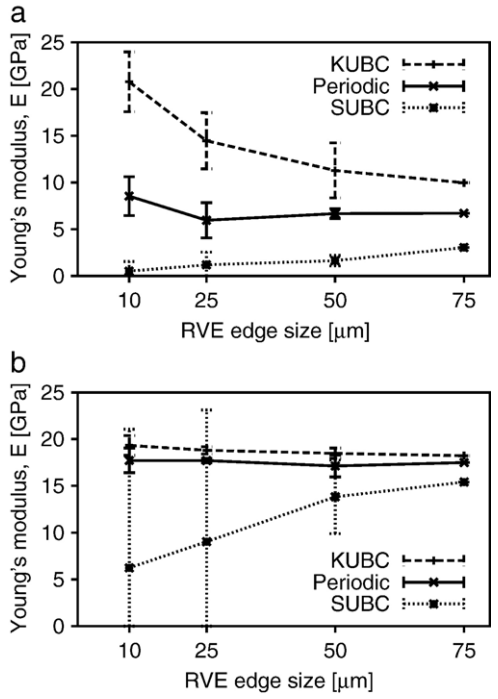

Fig. 8. Effect of kinematic, static and periodic boundary conditions, degree of hydration = 0.3 (a) and 0.9 (b), FEM, all with split nodes, wcr = 0.5.

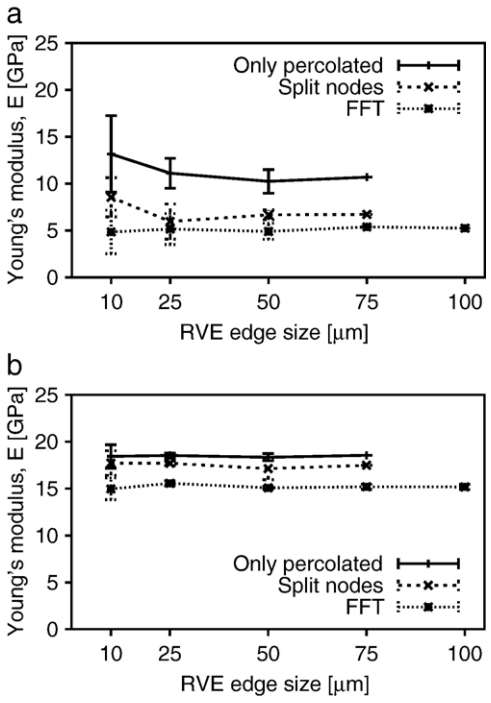

Fig. 9. Difference among percolated, split node mesh and FFT, degree of hydration = 0.3 (a) and 0.9 (b), periodic b.c. Note similar FFT results of various RVE sizes, wcr = 0.5.

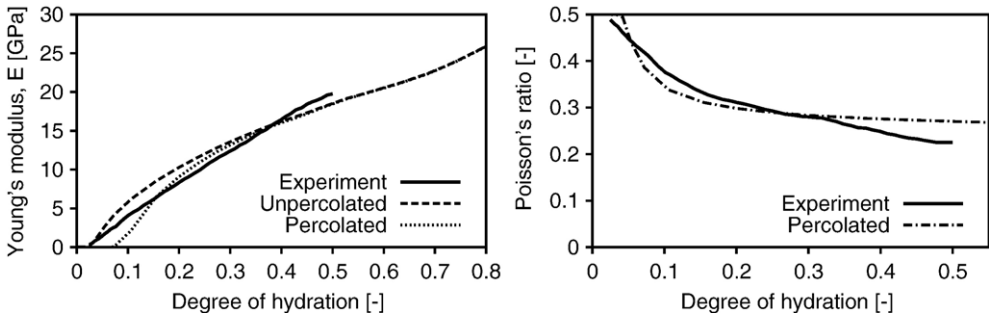

Fig. 10. Analytically predicted Young's modulus and Poisson's ratio using un/percolated volumetic fractions, wcr = 0.35.

hydration, the statistical homogeneity and isotropy become worse and the larger RVE may be necessary.

The results of the FFT method are theoretically exact, limited only by wanted precision of iterations in numerical implementation. Therefore, the difference with FEM shows an error caused by displacement approximations. Fig. 9 depicts the performance for the degree of hydration of 0.3 and 0.9. The highest E modulus yields a percolated RVE, followed by split nodes, converging to those in the FFT method. The FFT results testify that effective properties may be evaluated from several random realizations of considerably smaller RVEs [17], e.g., 10 μm. FEM exhibits poor approximation of displacements in such a small RVE; hence, a larger RVE improves the approximations rather than introducing new information from the cement microstructure.

4.2. White cement paste, wcr = 0.35

Boumiz et al. [5] measured acoustic wave velocities and the heat of hydration on a white cement paste of wcr = 0.35. Data were recalculated in terms of Young's modulus, Poisson's ratio and the degree of hydration. Our simulation ran on a 75 × 75 × 75 μm RVE with a 3 × 3 × 3 μm dissolution box and 1 μm voxel resolution. The results from the two-level analytical homogenization are in Fig. 10 for un- and percolated RVEs. The wcr of this paste corresponds roughly to 0.318, which is the value where the percolation threshold of solids coincides with the self-consistent scheme in terms of E modulus cut-off [3]. In experiment, the Poisson's ratio decreases from 0.5; therefore, the elastic properties of capillary water correspond to water-filled porosity (Table 1).

This white cement paste served for a study exploring how much the elastic properties are influenced when varying the resolution and voxel dissolution of the NIST model. An initial RVE of 25 × 25 × 25 μm was generated and consequently scaled two and three times. This corresponds to the voxel resolution of 1, 0.5 and 0.33 μm. In other words, there are three self-similar RVEs of 25 μm size with three above-mentioned resolutions. The dissolution neighborhood around a voxel may contain six or 26 possibly dissolved adjacent voxels, the latter corresponding to the full box of 3 × 3 × 3 voxels. The choice leads to a different RVE morphology and strongly influences hydration kinetics. Larger boxes than 3 × 3 × 3 voxels are physically unjustified since a dissolved phase cannot jump over a solid voxel [10]. Fig. 11 illustrates the results from FEM homogenization with split nodes and periodic boundary conditions, for three resolutions and both amount of possibly dissolved adjacent voxels. Although the results are different and not far apart, neither the voxel resolution nor the amount of six or 26 voxels influence the response dominantly. This suggests a conclusion that variant RVE arrangements from the NIST model at the same hydration degree and from the same cement paste lead to similar homogenized elastic properties.

4.3. Dense cement paste, wcr = 0.25

The dense microstructure of Kamali et al. [16], wcr = 0.25, was reconstructed in the size of 75 × 75 × 75 μm and hydrated

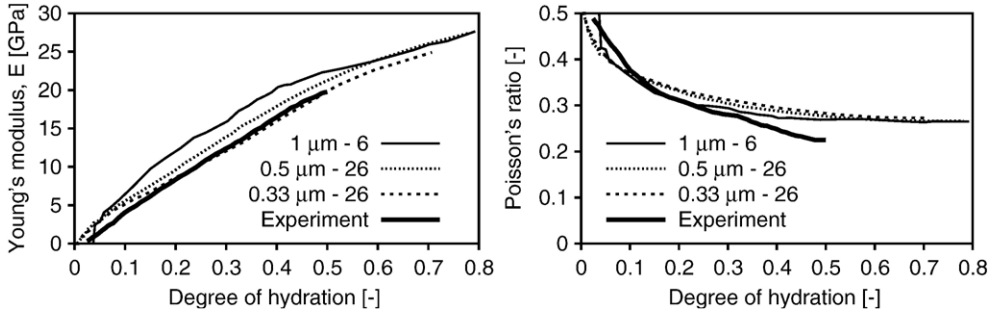

Fig. 11. E modulus and Poisson's ratio for the voxel resolution of 1, 0.5 and 0.33 μm and the amount of possibly dissolved voxels as six or 26, FEM–periodic b.c., RVE of 25 × 25 × 25 μm, wcr = 0.35.

with a 1 μm voxel resolution, in the 3×3×3 μm dissolution box. Fig. 12a shows the evolution of E modulus on the C–S–H level as obtained via the analytical method of Mori–Tanaka. Almost all initial C–S–H_{LD} is finally changed to the C–S–H_{HD} type which causes an increase of E modulus on this level. Fig. 12b displays the results on the cement paste level. The percolation threshold plays a significant role and, in this particular case, corresponds to the degree of hydration as low as 0.015. A low wcr means that a high portion of cement remains unhydrated in later stages due to unavailable pore space; therefore, the maximum degree of hydration attains approximately 0.62. The unhydrated clinker minerals boost the stiffness of the cement paste together with a higher portion of C–S–H_{HD}. The empirical formula of Eq. (9) is not well suited for the middle hydration period, as observed in Fig. 12b.

Fig. 13 demonstrates the evolution of Young's modulus for RVE sizes of 50 and 75 μm under periodic b.c. In early ages, the FFT homogenization on the 75×75×75 RVE predicts a higher E modulus than FEM which means that there is an excessive amount of split nodes. The difference between 50 and 75 μm sizes is again not significant for the whole hydration period, suggesting that 50 μm might be considered as reasonable minimum size. When the initial unpercolated RVE entered FEM homogenization, the E modulus would already begin at 26.2 GPa instead of 0.001 GPa, which illustrates the significance of percolation and the split node algorithm.

The apparent moduli were explored again on RVEs of 10, 25, 50 and 75 μm. Five randomly generated and hydrated samples were used for each size, having the same initial parameters of the NIST program as in the last simulation. Fig. 14 shows the effect of boundary conditions on apparent elastic properties for the hydration degrees of 0.3 and 0.62, respectively. The widest 95% confidence level was found for the static uniform boundary condition, the other b.c. are comparable in the scatter. The hydration degree of 0.3, which corresponds to the capillary porosity fraction of 23.4%, requires rather larger RVE, as evident from the fluctuation of mean values. A porosity fraction of 4.4% is reached at the degree of hydration of 0.62, which means that the contrast of elastic properties is reduced in terms of their volume fractions; therefore, different b.c. lead to similar results (Fig. 14b).

Fig. 15 displays the difference among percolated mesh, the split nodes mesh and the FFT method for two hydration degrees. All three configurations with periodic boundary conditions are close in a well-hydrated RVE while for a lower hydration degree the results from both meshes are different. The

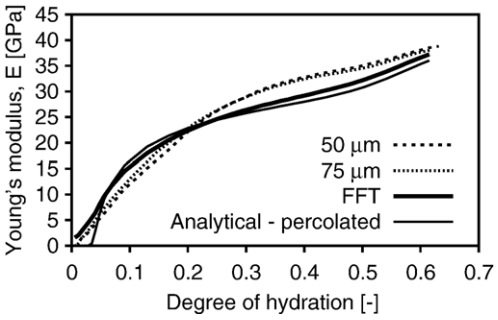

Fig. 13. Effect of RVE size on E modulus, FEM–periodic b.c., split nodes, FFT. Comparison with analytical homogenization from percolated RVE, wcr = 0.25.

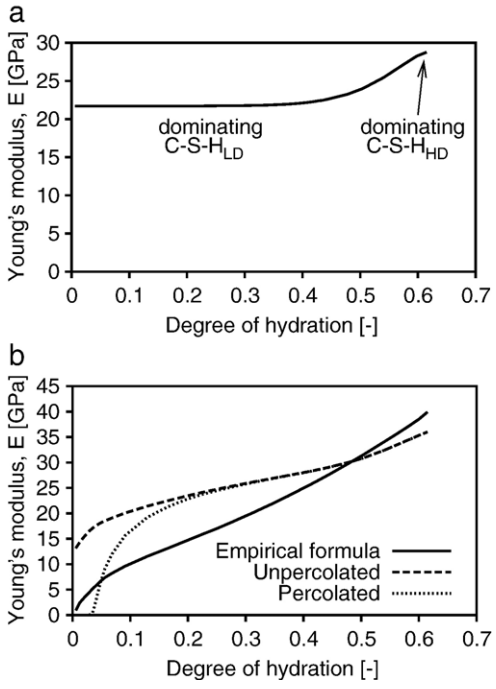

Fig. 12. Young's modulus predicted analytically (a) on the C–S–H level by the Mori–Tanaka method, (b) on the cement paste level by the self consistent scheme, wcr = 0.25.

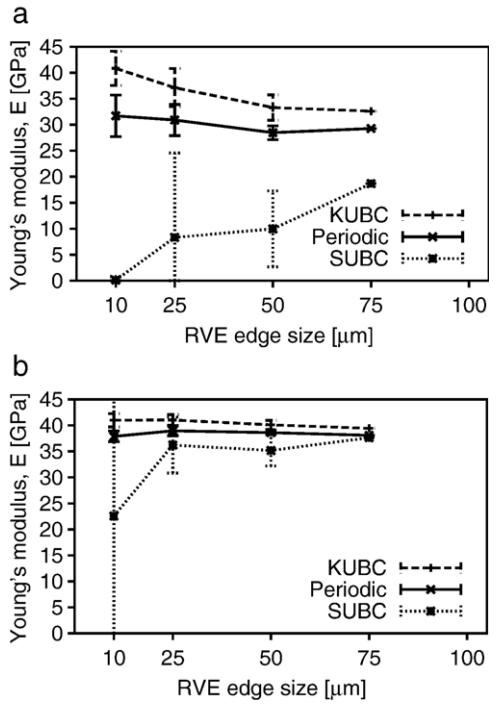

Fig. 14. Effect of kinematic, static and periodic boundary conditions, degree of hydration = 0.3 (a) and 0.62 (b), FEM, split nodes, wcr = 0.25.

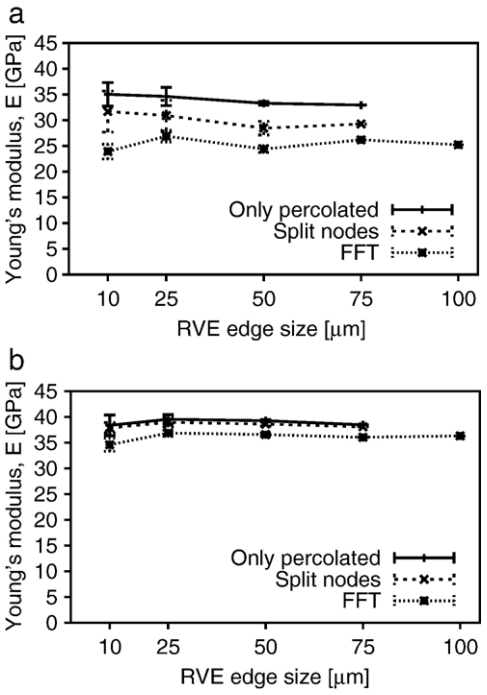

Fig. 15. Difference among percolated, split node mesh and FFT, degree of hydration = 0.3 (a) and 0.62 (b), periodic b.c., wcr = 0.25.

convergence of apparent moduli was tested on the $100 \times 100 \times 100$ μm RVE by means of the FFT homogenization. The maximal relative difference 0.6% between 50 and 100 μm was found in Young's modulus during the FFT homogenization. This suggests that the RVE of 50 μm edge is appropriate at least after the degree of hydration of 0.3.

5. Conclusion

This paper has presented a combination of the NIST cement hydration model and the linear elastic homogenization approach. Commonly used chemical reactions originating in the cement chemistry together with additional parameters were employed to reconstruct a digital image of hydrating cement paste. The NIST model was enhanced for prediction of two types of C–S–H, based on the confinement theory. Percolation of solids, i.e., their connectivity, is the key for proper simulation of early age elastic properties. Otherwise, the micromechanical models predict a stiffer response of RVE at that period.

Two-level analytical homogenization was extended to early ages, considering the percolation of solids. Validated wcrs in the range from 0.25 to 0.5 testify that Young's moduli are underestimated above wcr = 0.318 and vice versa, using the combination of the Mori–Tanaka and the self-consistent scheme [3].

The percolation concept was further extended with split nodes, minimizing stress concentration problems and allowing simple tri-linear approximation of displacements in the FEM. Kinematic, static and periodic boundary conditions were applied in order to explore the role of RVE size on apparent elastic properties. The periodic boundary conditions were found as the most appropriate for the following reasons: small bias of results of random realizations and excellent results even for small RVEs. In validated wcrs, a RVE edge size of 50 μm seems to be reasonable for determination of elastic properties via FEM.

The FFT-based homogenization served as an indicator of FEM displacement approximations. The FEM with split nodes on percolated RVEs yields similar values to FFT results in all validated wcrs except small RVEs, e.g., 10 μm. Such small RVEs were found reasonable for the FFT method since the solution is limited only by numerical precision, not by the selection of displacement approximations. If FEM used higher approximation functions, smaller RVE would also be reasonable.

All homogenization methods testify that the common assumption of linearity between hydration degree and E modulus is appropriate only for a wcr higher than approximately 0.35. Bellow that, the evolution of the E modulus has a concave shape, similar to the square root function.

Acknowledgement

We gratefully acknowledge the financial support from the Ministry of Education, Youth and Sports (MSM 6840770003-Algorithms for computer simulation and application in engineering), fruitful discussions with J. Zeman and M. Jirásek, the help of M. Wierer for the FFT implementation. D.P. Bentz and E.J. Garboczi are acknowledged for the NIST cement hydration model.

References

[1] F.G. Bell, A survey of the engineering properties of some anhydrite and gypsum from the north and midlands of England, Eng. Geol. 38 (1–2) (1994) 1–23.
[2] D.P. Bentz, CEMHYD3D: A Three-Dimensional Cement Hydration and Microstructure Development Modelling Package. Version 2.0, National Institute of Standards and Technology, Gaithersburg, 2000.
[3] O. Bernard, F.-J. Ulm, E. Lemarchand, A multiscale micromechanics hydration model for the early-age elastic properties of cement-based materials, Cem. Concr. Res. 33 (9) (2003) 1293–1309.
[4] H.J. Böhm, W. Han, Comparisons between three-dimensional and two dimensional multi-particle unit cell models for particle reinforced metal matrix composites, Model. Simul. Mater. Sci. Eng. 9 (2) (2001) 47–65.
[5] A. Boumiz, C. Vernet, F.C. Tenoudji, Mechanical properties of cement pastes and mortars at early ages: evolution with time and degree of hydration, Adv. Cem. Based Mater. 3 (3–4) (1996) 94–106.
[6] G. Constantinides, F.-J. Ulm, The effect of two types of C–S–H on the elasticity of cement-based materials: results from nanoindentation and micromechanical modeling, Cem. Concr. Res. 34 (1) (2004) 67–80.
[7] W.J. Drugan, J.R. Willis, A micromechanics-based nonlocal constitutive equation and estimates of representative volume element size for elastic composites, J. Mech. Phys. Solids 44 (4) (1996) 497–524.
[8] G. Fagerlund, Relations between the strength and the degree of hydration or porosity of cement paste, cement mortar and concrete, Cementa Report T87023, Danderyd, 1987.
[9] E.J. Garboczi, Finite Element and Finite Difference Programs for Computing the Linear Electric and Elastic Properties of Digital Images of Random Materials, National Institute of Standards and Technology, Gaithersburg, 1998.
[10] E.J. Garboczi, D.P. Bentz, The effect of statistical fluctuation, finite size error, and digital resolution on the phase percolation and transport

properties of the NIST cement hydration model, Cem. Concr. Res. 31 (10) (2001) 1501–1514.
[11] A.A. Gusev, Representative volume element size for elastic composites: a numerical study, J. Mech. Phys. Solids 45 (9) (1997) 1449–1459.
[12] C.-J. Haecker, E.J. Garboczi, J.W. Bullard, R.B. Bohn, Z. Sun, S.P. Shah, T. Voigt, Modeling the linear elastic properties of Portland cement paste, Cem. Concr. Res. 35 (10) (2005) 1948–1960.
[13] R. Hill, Theory of mechanical properties of fiber-strengthened materials: III. Self-consistent model, J. Mech. Phys. Solids 13 (1965) 189–198.
[14] C. Huet, Application of variational concepts to size effects in elastic heterogeneous bodies, J. Mech. Phys. Solids 38 (1990) 813–841.
[15] H.M. Jennings, A model for the microstructure of calcium silicate hydrate in cement paste, Cem. Concr. Res. 30 (1) (2000) 101–116.
[16] S. Kamali, M. Moranville, E.G. Garboczi, S. Pren, B. Grard, Hydrate dissolution influence on the Young's modulus of cement paste, in: Li, et al., (Eds.), Proc. Fracture Mechanics of Concrete Structures (FraMCoS-V), Ia-FraMCos, Vail, 2004.
[17] T. Kanit, S. Forest, I. Galliet, V. Mounoury, D. Jeulin, Determination of the size of the representative volume element for random composites: statistical and numerical approach, Int. J. Solids Struct. 40 (13–14) (2003) 3647–3679.
[18] J.C. Michel, H. Moulinec, P. Suquet, Effective properties of composite materials with periodic microstructure: a computational approach, Comput. Methods Appl. Mech. Eng. 172 (1999) 109–143.
[19] T. Mori, K. Tanaka, Average stress in matrix and average elastic energy of materials with misfitting inclusions, Acta Metall. 21 (5) (1973) 1605–1609.
[20] H. Moulinec, P. Suquet, A FFT-based numerical method for computing mechanical properties of composite materials from images of their microstructure, in: R. Pyrz (Ed.), Microstructure-Property Interactions in Composite Materials, Kluwer Academic Publishers, Dordrecht, 1995, pp. 235–246.
[21] I.G. Richardson, The nature of C–S–H in hardened cements, Cem. Concr. Res. 29 (8) (1999) 1131–1147.
[22] G. De Schutter, L. Taerwe, Degree of hydration-based description of mechanical properties of early age concrete, Mat. Struct. 29 (7) (1996) 335–344.
[23] V. Šmilauer, Z. Bittnar, Effects of representative cube size on the simulation of Portland cement hydration in CEMHYD3D model, in: J. Walraven, J. Blaauwendraad, T. Scarpas, B. Snijder (Eds.), 5th International PhD Symposium in Civil Engineering, A. A. Balkema Publishers, 2004, pp. 581–587.
[24] Z. Sun, G. Ye, T. Voigh, S.P. Shah, K. van Breugel, Microstructural as pects of cement hydration–ultrasonic waves and numerical simulation, in: J. Walraven, J. Blaauwendraad, T. Scarpas, B. Snijder (Eds.), 5th International PhD Symposium in Civil Engineering, A. A. Balkema Publishers, 2004, pp. 971–979.
[25] N. Takano, M. Zako, F. Kubo, K. Kimura, Microstructure-based stress analysis and evaluation for porous ceramics by homogenization method with digital image-based modeling, Int. J. Solids Struct. 40 (5) (2003) 1225–1242.
[26] P.D. Tennis, H.M. Jennings, A model for two types of calcium silicate hydrate in the microstructure of Portland cement pastes, Cem. Concr. Res. 30 (6) (2000) 855–863.
[27] S. Torquato, Modeling of physical properties of composite materials, Int. J. Solids Struct. 37 (1–2) (2000) 411–422.
[28] S. Torquato, Random Heterogeneous Materials, Microstructure and Macroscopic Properties, Springer-Verlag, New York, 2001.
[29] J.M. Torrenti, F. Benboudjema, Mechanical threshold of cementitious materials at early age, Mat. Struct. 38 (2005) 299–304.
[30] K. Velez, S. Maximilien, D. Damidot, G. Fantozzi, F. Sorrentino, Determination by nanoindentation of elastic modulus and hardness of pure constituents of Portland cement clinker, Cem. Concr. Res. 31 (4) (2001) 555–561.
[31] G. Ye, Z. Sun, T. Voigt, K. van Breugel, S.P. Shah, A micromechanical model for characterization of cement paste at early age validated with experiments, International Symposium: Advances in Concrete through Science and Engineering, Evanston, 2004.
[32] A. Zaoui, Continuum Micromechanics: Survey, J. Eng. Mech. 128 (8) (2002) 808–816.
[33] J. Zeman, M. Šejnoha, Numerical evaluation of effective elastic proper ties of graphite fiber tow impregnated by polymer matrix, J. Mech. Phys. Solids 49 (1) (2001) 69–90.